The European Large Area ISO Survey: optical identifications of 15-μm and 1.4-GHz sources in N1 and N2

Article (Published Version)

Mon. Not. R. Astron. Soc. **358,** 333–340 (2005) doi:10.1111/j.1365-2966.2005.08725.x

The European Large Area *ISO* Survey: optical identifications of 15-μm and 1.4-GHz sources in N1 and N2

E. A. Gonzalez-Solares,[1⋆] I. Perez-Fournon,[2] M. Rowan-Robinson,[3] S. Oliver,[4] M. Vaccari,[5] C. Lari,[6] M. Irwin,[1] R. G. McMahon,[1] S. Hodgkin,[1] P. Ciliegi,[7] S. Serjeant[8] and C. J. Willott[9]

[1]*Institute of Astronomy, University of Cambridge, Madingley Road, Cambridge CB3 0HA*
[2]*Instituto de Astrofísica de Canarias, C/Via Lactea, s/n, La Laguna E38200, Spain*
[3]*Astrophysics Group, Blackett Laboratory, Imperial College of Science, Technology & Medicine, Prince Consort Road, London SW7 2BZ*
[4]*Astronomy Centre, Department of Physics and Astronomy, University of Sussex, Falmer, Brighton BN1 9QJ*
[5]*Dipartamento di Astronomia, Universitai Padova, Vicolo Osservatorio 5, I-35122 Padova, Italy*
[6]*Istituto di Radioastronomia, Via P. Gobetti 101, Bologna 40129, Italy*
[7]*Osservatorio Astronomico di Bologna, Via Ranzani 1, 40127 Bologna, Italy*
[8]*Centre for Astrophysics and Planetary Science, School of Physical Sciences, University of Kent, Canterbury, Kent CT2 7HR*
[9]*Herzberg Institute of Astrophysics, National Research Council, 5071 West Saanich Road, Victoria, B. C. V9E 2E7, Canada*

Accepted 2004 December 7. Received 2004 October 26

ABSTRACT

We present the multiwavelength properties and catalogue of the 15 μm and 1.4 GHz radio sources detected in the European Large Area *ISO* Survey (*ELAIS*) areas N1 and N2. Using the optical data from the Wide Field Survey we use a likelihood ratio method to search for the counterparts of the 1056 and 691 sources detected at 15 μm and 1.4 GHz, respectively, down to flux limits of $S_{15} = 0.5$ mJy and $S_{1.4\,\mathrm{GHz}} = 0.135$ mJy. We find that ∼92 per cent of the 15 μm *ELAIS* sources have an optical counterpart down to $r' = 24$. All mid-infrared (IR) sources with fluxes $S_{15} \geqslant 3$ mJy have an optical counterpart. The magnitude distribution of the sources shows a well-defined peak at relatively bright magnitudes $r' \sim 18$. The mid-IR-to-optical and radio-to-optical flux diagrams are presented and discussed in terms of actual galaxy models. About 15 per cent of the sources are bright galactic stars; of the extragalactic objects ∼65 per cent are compatible with being normal or starburst galaxies and ∼25 per cent active galactic nuclei (AGNs). Objects with mid-IR-to-optical fluxes larger than 100 are found, comprising ∼20 per cent of the sample. We suggest that that these sources are highly obscured luminous and ultraluminous starburst galaxies and AGNs.

Key words: stars: formation – galaxies: evolution – galaxies: starburst – cosmology: observations – infrared: galaxies.

1 INTRODUCTION

The *Infrared Space Observatory* (*ISO*, Kessler et al. 1996) was the second infrared (IR) space mission and the first mission to be used as an IR observatory, providing a great improvement in sensitivity over the *IRAS* mission. A large fraction of the observatory time was spent in performing extragalacitc surveys. Their major goal was to characterize the sources detected in the mid-IR and responsible for the cosmic IR background. In the mid-IR the *ISOCAM* camera (Cesarsky et al. 1996) was $\sim 10^3$ times more sensitive and had 60 times higher spatial resolution than *IRAS*. In the far-IR with ISOPHOT (Lemke et al. 1996), the improvement in sensitive is much lower, but the extension to longer wavelengths (175 μm) was of substantial benefit. The *ISO* surveys have taken advantage of these improvements to provide a view of the IR universe at redshifts $z \gtrsim 0.5$ (see e.g. Genzel & Cesarsky 2000).

Mid-IR surveys in the 15-μm wavelength regime, are sensible to emission from hotter sources such as active galactic nuclei (AGNs) or luminous starbursts, they are also sensible to emission from normal galaxies. The nature of the mid-IR sources has been studied, however, only in small fields. Surveys in these bands include the *Hubble Deep Field* (HDF) surveys in the North and South (Aussel et al. 1999; Oliver et al. 2002), the Canada–France Redshift Survey (Flores et al. 1999) and the ISOCAM guaranteed time extragalactic surveys in the Lockman Hole (e.g. Fadda et al. 2002).

The European Large Area *ISO* survey (ELAIS, Oliver et al. 2000) was the largest Open Time programme on *ISO*. This project surveyed

⋆E-mail: eglez@ast.cam.ac.uk

12 deg^2, divided into four main fields, three in the north (N1, N2, N3) and one in the south (S1). The main survey bands used were 6.7, 15, 90 and 170 μm. The ISOCAM camera was used for the shorter wavelengths while the ISOPHOT camera was used for the longer ones. The final analysis of the 15-μm data has been recently completed in the northern (Vaccari et al. 2005) and southern (Gruppioni et al. 2002) areas.

Pozzi et al. (2003) discuss the identification of a sample of 43 ELAIS sources detected at 15 μm in one of the small southern fields (S2; 0.12 deg^2), finding an optical identification rate of about 90 per cent to magnitude $I = 21$. They also show that most of their extragalactic objects with spectroscopy observations (70 per cent of the total sample) are normal spiral or starburst galaxies at a median redshift of $z \sim 0.2$. In a similar way, La Franca et al. (2004), present the optical catalogue of 406 sources detected at 15 μm in the ∼4 deg^2 of ELAIS S1. Down to a magnitude limit of $R \sim 23$ they find an optical counterpart for ∼82 per cent of the sources and from their spectroscopic observations they find that ∼75 per cent of the extragalactic objects are starburst galaxies and ∼22 per cent are AGNs.

This paper presents the optical identification of the 1056 mid-IR and 691 radio sources in the N1 and N2 areas. These are the two main survey areas in the northern observations, comprising a total of 5.7 deg^2. This work thus extends those carried out by Pozzi et al. (2003) and La Franca et al. (2004) to a larger area and ∼2 mag deeper multiband optical observations. The final ELAIS bandmerge catalogue is presented in Rowan-Robinson et al. (2004).

Optical imaging is essential to study the properties of the sources detected. Section 2 presents the optical observations carried out in these areas as well as the reduction steps and data products. Section 3 describes the mid-IR and radio catalogues used. Owing to the large error ellipses of the mid-IR detections, typically several seconds of arc, it is necessary to carry out a detailed process of identification. As more than one optical source can be inside those ellipses, a method which provides the likelihood of each counterpart to be the true association is needed. Section 4 discusses the actual procedure to determine the optical counterparts of the sources, while Sections 5 and 6 describe the optical properties of the sources.

2 THE OPTICAL CATALOGUES

To identify the mid-IR sources with optical objects we use the data from the Wide Field Survey (WFS, McMahon et al. 2001). This survey has been carried out using the Wide Field Camera (WFC) on the 2.5-m Isaac Newton Telescope (INT) on the Observatorio del Roque de Los Muchachos (La Palma). The WFC is formed by four 4k × 2k CCDs. The arrays have 13.5 μm pixel corresponding to 0.33″ pixel^{-1} at the telescope prime focus and each one covers an area on sky of 22.8 × 11.4 arcmin. The total sky coverage per exposure for the array is therefore 0.29 deg^2. Gaps between detectors are typically 20 arcsec. Chip 3 is slightly vignetted in one corner. Optical observations described below are carried out considering the WFC as a 3-CCD camera, allowing for a 10 per cent overlap between adjacent pointings for photometric purposes. Therefore the area not observed in each pointing owing to the chip gaps is about 12 arcmin^2. However, the spatial source density of ELAIS and radio sources is not high enough to make this effect important for the process of identification.

The WFS surveyed ∼200 deg^2 in different well-known regions of sky with data at other wavelengths. The N1 and N2 ELAIS regions were also included. The survey consists of single 600-s exposures in five bands: U, g', r', i' and Z to magnitude limits of 23.4, 24.9, 24.0, 23.2 and 21.9, respectively (Vega, 5σ for a point-like object), i.e. about 1 mag deeper than the Sloan Digital Sky Survey (SDSS; York et al. 2000). A total of 108 pointings were done in N1 and N2, covering a total area of 18 deg^2. Typical seeing is about 1.0–1.2 arcsec. The data are processed by the Cambridge Astronomical Survey Unit (CASU) as described in Irwin & Lewis (2001) and we provide here a short description of the reduction steps. The data are first debiased (full two-dimensional bias removal is necessary). Bad pixels and columns are then flagged and recorded in confidence maps, which are used during catalogue generation. The CCDs are found to have significant non-linearities so a correction using look-up tables is then applied to all data. Flatfield images in each band are constructed by combining several sky flats obtained in bright sky conditions during the twilight. Exposures obtained in the i' and Z bands show a significant level of fringing (±2 and ±6 per cent of sky, respectively). In order to remove this effect, master fringe frames are created by combining all the science exposures for each band. These fringe frames are then subtracted from the object exposures. After this removal, the fringing level is reduced to ±0.2 and ±0.4 per cent of sky in the i' and Z bands, respectively. Finally an astrometric solution starts with a rough WCS based on the known telescope and camera geometry and is the progressively refined using the Guide Star Catalogue for a first pass and the APM or PMM catalogues for a final pass. The WFC field distortion is modelled using a zenithal equidistant projection (ZPN; Greisen & Calabretta 2002). The resulting internal astrometric precision is better than 100 mas over the whole WFC array (based on intercomparison of overlap regions). Global systematics are limited by the precision of the APM and PMM astrometric catalogue systems and are at the level of 300 mas. The object detection is performed in each band separately using a standard APM-style object detection and parametrization algorithm. Standard aperture fluxes are measured in a set of apertures of radius $r/2, r, \sqrt{2}r, 2r, 2\sqrt{2}r$ where $r =$ 3.5 pixel and an automatic aperture correction (based on the average curve-of-growth for stellar images) is applied to all detected objects.

Photometric calibration is done using series of Landoldt standard stars (Landolt 1992) with photometry in the SDSS system. For each night a zero-point in each filter is derived. For photometric nights the calibration over the whole mosaic has an accuracy of 1–2 per cent. During non-photometric nights, in otherwise acceptable observing conditions, we find that the derived zero-point systematic errors can be up to 10 per cent or more. Although the pipeline usually successfully flags such nights as non-photometric it still leaves open the problem of what to do about tracking the varying extinction during these nights.

All calibration is by default corrected for the mean atmospheric extinction at La Palma during pipeline processing (0.46 in U, 0.19 in g', 0.09 in r' and 0.05 in i' and Z). As adjacent camera pointings overlap by several square arcminutes sources in these overlapping regions can be used as magnitude comparison points. However, to use overlapping and hence in general, different CCDs, requires that any repeatable systematics owing to, for example, slight differences in the colour equations for each CCD, are first corrected for. Correcting for these is a three stage process. First the twilight flatfields are used to gain-correct each CCD on to a common system. However, as the twilight sky is significantly bluer than most astronomical objects, a secondary correction is made using the measured dark sky levels in each CCD for each filter to provide a correction more appropriate for the majority astronomical object. These corrections, unsurprisingly, are negligible for passbands on the flat part of the generic CCD response curves such as g' and r', and amount to

1–2 per cent for the i' and Z passbands. The measured dark sky values for the U band were also consistent with zero correction though with less accuracy owing to the low sky levels in the U-band images. Finally any residual offsets between the CCDs are checked for each survey filter using the mean offset between adjacent pointings on photometric survey nights. The only filters requiring significant adjustments to the individual CCD zero-points at this stage are CCD3 for U (-3 per cent) and CCD1 for Z ($+3$ per cent).

Data from non-photometric nights can now be calibrated in one of two ways: the overlap regions between pointings can be used to directly tie in all the frames on to a common system, with extra weighting given to data taken from photometric nights; the stellar locus in various two-colour diagrams (in regions of low unchanging extinction like these) can be used to compare colours from all the passbands by cross-correlating the loci between any of the pointings. The colour–colour loci cross-correlations (actually made from a smoothed Hess-like version of the diagrams) give results accurate to better than ± 3 per cent and can be used in conjunction with the overlap results to give overall photometry for the survey to the level of $\approx$2 per cent. The final products include astrometrically calibrated images as well as morphologically classified merged multicolour catalogues, publically available from the WFS web page (http://www.ast.cam.ac.uk/$\sim$wfcsur/index.php).

For the purpose of this work, we have also carried out the object detection in the r'-band images using SExtractor (Bertin & Arnouts 1996). As well as providing a independent check for the extraction method used, it gives us an extense set of additional parameters. Aperture magnitudes from SExtractor are found to be in agreement with the ones obtained from the WFS pipeline. Therefore, together with the WFS aperture magnitudes we use MAG_BEST (which is defined as the best magnitude between an isophotal corrected magnitude and a adaptative aperture magnitude) as a measurement of the total magnitude in the r' band. The galaxy–star classification given by CLASS_STAR is also used to select point-like objects (defined to be CLASS_STAR >0.8).

As an additional test of our photometric calibration we have correlated the WFS catalogues with those from the SDSS First Data Release (Abazajian et al. 2003). The agreement between both magnitudes are within 4 per cent.

3 THE MID-INFRARED AND RADIO CATALOGUES

The final analysis of the 15-μm data using the Lari method (Lari et al. 2001) for the ELAIS northern fields has recently been completed (Vaccari et al. 2005). The two main northern fields N1 and N2 are centred at $16^{\rm h}10^{\rm m}01^{\rm s} + 54^\circ30'36''$ and $16^{\rm h}36^{\rm m}58^{\rm s} + 41^\circ15'43''$, respectively. We have obtained a sample of 1056 sources (490 in N1 and 566 in N2) to a 5σ flux limit of 0.45 mJy. This catalogue includes sources detected in deeper observations (in particular, the central $40' \times 40'$ N2 area has been observed three times) so this flux limit is not homogenous over the whole survey area.

As part of the multiwavelength follow-up observations carried out in these regions Ciliegi et al. (1999) have conducted a survey at 20 cm using the VLA in its C configuration, covering 4.22 deg^2 in the N1, N2 and N3 areas. They detect a total of 867 sources (362 in N1, 329 in N2 and 176 in N3) above a flux limit of 0.135 mJy in the deeper observations or 1.15 mJy over the shallower ones. We have selected sources for which we have optical data from the WFS (i.e. sources in N1 and N2). Multicomponent sources (flagged in the catalogue as 'A', 'B' or 'C' components) have been removed and only the calculated central position considered ('T' in the catalogue).

4 OPTICAL IDENTIFICATIONS OF ELAIS SOURCES

As shown in Lari et al. (2001), the positional errors in RA and Dec. for the ELAIS sources result from the combination of three quantities: the finite spatial sampling ($\sigma_{\rm s}$), the reduction method ($\sigma_{\rm r}$) and the pointing accuracy ($\sigma_{\rm P}$). The simulation work carried out in the ELAIS fields yield the following relations:

$$\sigma_{\rm s+r}({\rm RA}) = 1.00 + 17.17 \times {\rm e}^{(-0.57\times {\rm S/N})} \quad (1)$$

$$\sigma_{\rm s+r}({\rm Dec.}) = 1.06 + 1.21 \times {\rm e}^{(-0.16\times {\rm S/N})}. \quad (2)$$

These equations have been used to estimate the positional errors owing to the mapping and reduction method as a function of signal-to-noise (S/N) ratio of each source.

The errors introduced by uncertainties in the ISOCAM pointing have been estimated by correlating the *ISO* sources with the USNO catalogue of optical objects (Monet 1998). For each raster, both catalogues have been correlated using a maximum search distance of 12 arcsec. The *median* of the offsets values for all the *ISO*-USNO associations have been calculated, $\sigma_{\rm P}({\rm RA})$, $\sigma_{\rm P}({\rm Dec.})$. Each source position has then been corrected for the offset found for each raster. The final positional error is then

$$\sigma^2_{\rm RA} = \sigma^2_{\rm s+r}({\rm RA}) + \sigma^2_{\rm P}({\rm RA}) + 0.4^2 \quad (3)$$

$$\sigma^2_{\rm Dec.} = \sigma^2_{\rm s+r}({\rm Dec.}) + \sigma^2_{\rm P}({\rm Dec.}) + 0.4^2, \quad (4)$$

where $\sigma = 0.4$ arcsec has been added to account for the optical errors.

The correlation between ELAIS 15-μm sources and optical objects has been carried out using a likelihood ratio method (Sutherland & Saunders 1992), similar to the one which has been successfully applied to the identification of 15-μm sources detected by *ISO* in the HDF-N by Mann et al. (1997).

The probability that an optical object of magnitude m is the true counterpart of a source with an error ellipse defined by its major axis, σ_1, and minor axis, σ_2, separated a distance r is given by

$$\mathcal{L} = \frac{Q(m)\exp(-r^2/2)}{2\pi\sigma_1\sigma_2 N(m)}, \quad (5)$$

where Q and N are the magnitude distributions of the sources and objects, respectively. The reliability of such identification is

$$\mathcal{R}_j = \frac{\mathcal{L}_j}{\sum_i \mathcal{L}_i + (1-Q)}. \quad (6)$$

The identification process is carried out as follows. For each ELAIS 15-μm source, all optical objects within a distance of 20 arcsec are selected. This list is our candidate list. For each object in our candidate list we calculate the values of the likelihood and reliability as given by equations above. The likelihood value (equation 5) gives us the probability that a candidate is the true optical counterpart of the source; but it only provides information about the probability of each candidate being the correct counterpart. The reliability (equation 6) provides information about the number of candidates with high likelihood values. A candidate will have large values of likelihood and reliability if it is the only probable counterpart of a source. In case where there are multiple probable counterparts (in the sense of high likelihood), they all will have low reliability values.

A candidate is selected to be the correct optical identification of a ELAIS source when $\mathcal{L} > 0.8$. Sources for which no candidates meet this requirement are flagged as blank fields and represent $\sim$8 per cent of the total sample. Sources for which there are more than one candidate meeting this requirement, and have low values of reliability,

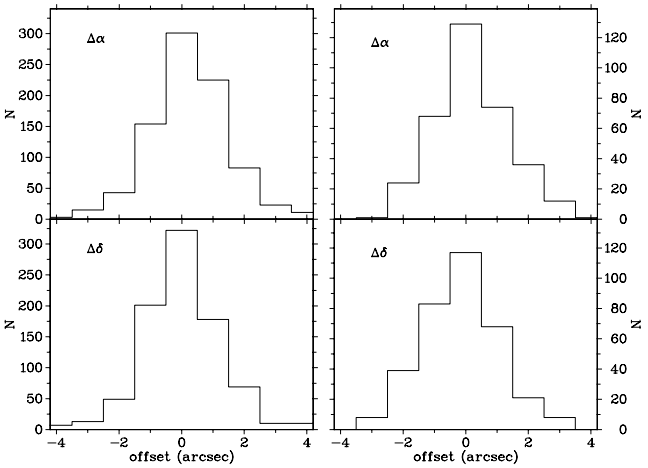

Figure 1. Offsets between 15 μm and optical positions (left) and between radio and optical positions (right).

are flagged as having multiple possible counterpart and represent ∼8 per cent of the sample. Finally, bright galactic stars, the majority of which are saturated in the WFS CCD data are also flagged. They represent ∼15 per cent of the sample. Fig. 1 (left) shows the offsets between *ISO* and optical identifications, excluding saturated stars. Uncertainties are well fitted by a Gaussian distribution of $\sigma \sim 1$ arcsec.

Optical identification of the ELAIS radio sources detected in the N1 and N2 areas is carried out using a similar procedure. In this case the radio catalogue provides measurements of the positional errors, so these are used in our likelihood ratio algorithm. An optical counterpart is found for 389 out of the 691 sources, i.e. 44 per cent are blank fields. The offsets between the radio and their optical positions are shown in Fig. 1. This provides a confirmation of the good accuracy of the astrometry of the 15-μm sources.

Fig. 2 shows some example finding charts of sources detected at 15 μm. These charts are 30 arcsec×30 arcsec in size and have been extracted from the r'-band images. Also shown a 3-arcsec radius circle centred on the *ISO* position. As shown in Section 5 a large fraction of the sources are associated with bright galaxies. An example of sources with more than one plausible counterpart is given by J163636.2+411049. The most likely counterpart is an object with $r' = 21.8$ at a distance of 1.1 arcsec from the *ISO* position. Its likelihood is 0.988 and reliability is 0.773. There is another source of $r' = 23.0$ separated 2 arcsec from the *ISO* position with likelihood 0.960 and reliability 0.227. We choose the first one as the optical counterpart (based on higher values of likelihood and reliability) of the *ISO* source and flag it as having more than one plausible counterpart. Examples of these are also J160347.5+544552 and J160721.6+535437.

There are four ELAIS sources which have been merged in the final analysis 15-μm catalogue (see Fig. 3). Both possible counterparts are given in the optical identification catalogue and the 15-μm flux is assigned to both.

The table of optical identifications is available online at http://www.blackwellpublishing.com/products/journals/suppmat/MNR/MNR8725/MNR8725sm.htm, and also at the website of the author E. A. Gonzales-Solares at http://www.ast.cam.ac.uk/∼eglez/eid. Also included at the latter website are postage stamps for all the sources in the r' band (greyscale and contours) as well as multiband greyscale finding charts.

The format of the table is as follows.

Column 1. International Astronomical Unit name of the source. Sources are listed in RA order. Sources detected in N2 are listed after those detected in N1.

Column 2. *ISO* coordinates (J2000) of the sources.

Column 3. Coordinates (J2000) of the optical counterpart of the source.

Columns 4–8. Aperture magnitude in U, g', r', i' and Z bands (aperture of radius 3.5 pixel–1.16 arcsec).

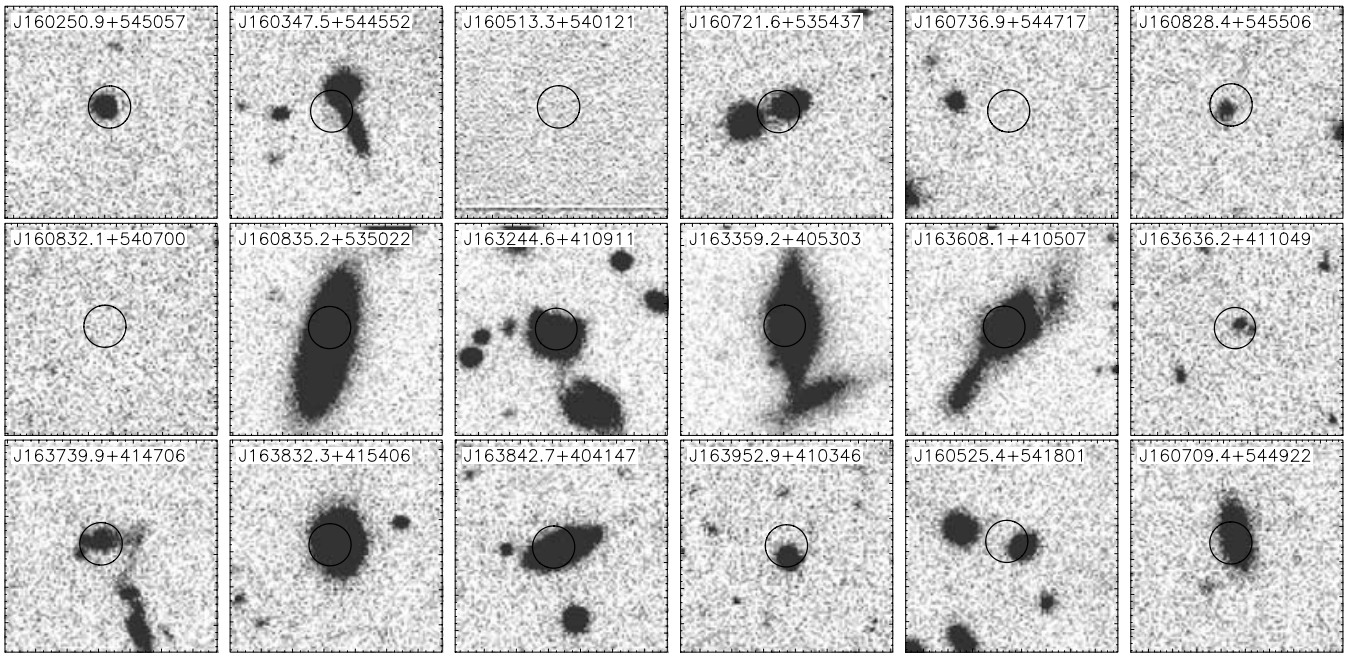

Figure 2. Example r'-band postage stamps of 15-μm detected sources. Each chart is 30 arcsec×30 arcsec in size.

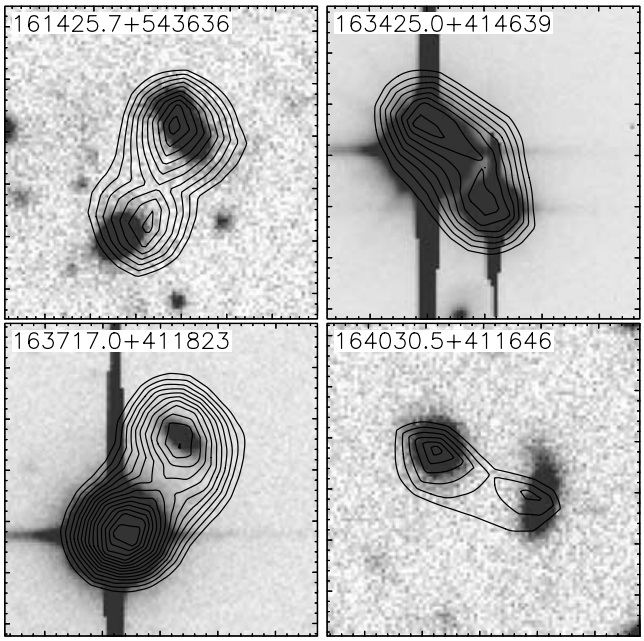

Figure 3. Double sources merged in the ELAIS 15-μm catalogue. Mid-IR contours starting at 5 σ and increasing at steps of 1σ are shown plotted over the r'-band image. Each chart is 30 arcsec×30 arcsec in size.

Column 9. Total r'-band magnitude (SExtractor MAG_BEST parameter).

Columns 10–15. Errors in previous magnitudes.

Columns 16–21. Stellar classification as provided by WFS and SExtractor CLASS_STAR parameters. Objects with CLASS_STAR larger than 0.8 are classified as point-like in this work.

Columns 22–24. Distance, $\Delta\alpha$ and $\Delta\delta$ between the ELAIS source and the optical association.

Columns 25 and 26. Likelihood of the identification formatted as $\mathcal{L}/(1+\mathcal{L})$ and reliability.

Columns 27 and 28. Flux at 15 μm and S/N ratio.

Column 29. Optical flag code as follows. B1, source in a gap between chips or in the edge of a chip; B3, most likely optical identification when multiple counterparts; B4, blank field; B7, bright saturated star; B9, other plausible optical identification when multiple counterparts.

5 MAGNITUDE DISTRIBUTIONS

Fig. 4 shows the magnitude distribution of the optical counterparts of ELAIS 15-μm sources. The first peak at $r' \sim 12$–13 is caused by bright stars which are saturated in the WFS data. The second peak, owing to extra-galactic objects, is located at $r' = 18$. Most of the extragalactic sources are then associated with optically bright objects. A tail of faint objects is present at $r' > 20$.

To calculate the percentage of chance associations, especially at the faintest magnitudes, we have simulated four catalogues in each N1 and N2 regions by offsetting 20 arcsec in RA and Dec. from the *ISO* position in four directions. The likelihood ratio technique was used to associate the sources in these new catalogues in the same way as done for the real ones. The identifications obtained provide the distribution of chance associations. This percentage is ∼5 per cent for $r' \leqslant 20$ and increases to 20 per cent at $r' = 24$.

Fig. 4 also shows the magnitude distribution of point-like objects. About 16 per cent of the objects with magnitude $r' > 15$ are classified as point-like. Their magnitude distribution has a peak at $r' \sim 19$, a magnitude fainter than that for galaxies.

The magnitude distribution of radio sources is shown in Fig. 5. Unlike the distribution of mid-IR sources, the number of sources show an increase at fainter magnitudes. The number of point-like objects is very low (hatched histogram) but the reliability of the CLASS_STAR parameter in SExtractor decreases at faint magnitudes and fails at $r' \geqslant 23$.

6 OPTICAL TO INFRARED FLUXES

Fig. 6 shows the mid-IR to optical fluxes for the ELAIS sources. Stars have typically low mid-IR fluxes compared to their optical fluxes and are located in the region where their mid-IR flux is ten times smaller than their optical flux. Most of the extragalactic objects have mid-IR fluxes between 1 and 100 times their optical fluxes. According to models of IR galaxies previously published Rowan-Robinson (2001), galaxies whose IR emission is dominated by cirrus are located in the region $0 < \log S_{15}/S_{r'} < 1$. More IR 'active' galaxies, i.e. starbursts, AGN and Arp220-like objects are located in regions of mid-IR flux 10–100 times larger than their optical flux.

Optical colours can be used to discriminate between AGNs and galaxies. As Fig. 7 shows AGNs are typically 0.5 mag bluer than galaxies (and as shown in Fig. 7, about 1 mag fainter). There is a population of point-like objects with galaxy-like colours, presumable highly obscured. Their overall spectra can be well fitted by a galaxy spectral energy distribution (SED) (Rowan-Robinson et al. 2004).

The radio to optical flux ratio versus magnitude and versus optical colour are shown in Figs 8 and 9 for the 1.4-GHz sources with optical counterpart. Those sources which show emission at 15 μm are also marked with black symbols. Most of the 15 μm–radio coincidences are objects with magnitudes $15 < r' < 20$ for which the cirrus component is the most plausible source of the IR and radio emission.

Attending to their radio, mid-IR and optical properties (see also Fig. 10) the bulk of the 15-μm sources (those with $0 < \log S_{15}/S_{r'} < 2$) can be explained as a mixture of cirrus-dominated galaxies and starburst with smaller fractions of Arp 220-like objects and AGN.

Table 1 lists the sources without optical counterpart which do have a radio identification.

6.1 Population with large IR-to-optical flux ratio

Fig. 6 also shows the existence of a population of objects with extreme mid-IR to optical fluxes and faint optical magnitudes.

Table 1. ELAIS blank fields with a radio source nearer than 3 arcsec from the *ISO* position. Fluxes are given in mJy.

Name	*ISO* Coords (J2000)	$S_{15\,\mu m}$	$S_{20\,cm}$
J160734.3+544216	16 07 34.40 +54 42 15.6	1.51 ± 0.19	0.37 ± 0.02
J163505.4+412508	16 35 05.71 +41 25 11.2	0.83 ± 0.09	0.38 ± 0.02
J163511.4+412255	16 35 11.54 +41 22 57.4	0.72 ± 0.09	0.94 ± 0.02

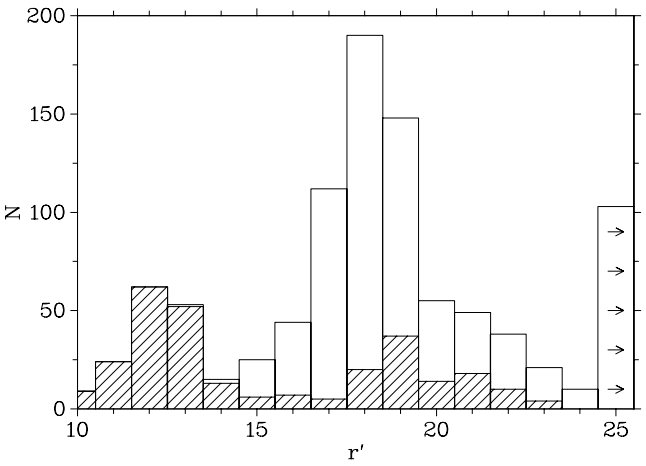

Figure 4. Magnitude distribution of 15-μm sources in ELAIS N1 and N2. Hatched histogram shows the distribution of point-like sources. Last bin, with right arrow symbols, represent the objects without an optical counterpart.

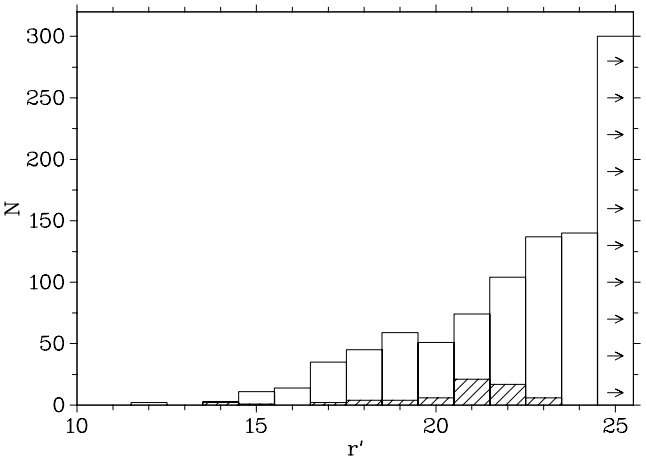

Figure 5. Magnitude distribution of 1.4-GHz radio sources in ELAIS N1 and N2. Hatched histogram shows the distribution of point-like sources. Last bin, with right arrow symbols, represent the objects without an optical counterpart.

The nature of this population can only be studied with detailed spectroscopic follow-up observations. Two of the point-like objects in this region of the diagram have spectroscopic redshifts. The object associated with ELAISC15_J164021.5+413925 has a 15-μm flux of $S_{15} = 2.98$ mJy, an optical magnitude of $r' = 20.3$ and a redshift $z = 0.60$ (Perez-Fournon et al., in preparation). Its luminosity is $L = 10^{11}\,L_{\odot}$. The second object is associated with ELAISC15_J163655.8+405909. It has a 15-μm flux of $S_{15} = 0.72$ mJy, an optical magnitude of $r' = 23.9$ and a redshift $z = 2.61$ (Willott et al. 2003). Its luminosity is $L = 10^{12}\ L_{\odot}$ ($H_0 = 65$, $\Omega_m = 0.3$, $\Lambda_0 = 0.7$).

Using IR models of starburst galaxies and AGN, and adding reddening (as modelled by Calzetti et al. 2000), we can explain the nature of this population. Objects with $\log\ S_{15}/S_{r'} > 2$ can be explained as luminous starburst galaxies, with luminosities $L \sim 10^{12}$ $L_{\odot}$, at redshifts $z \sim 0.7$ and reddening $A_v \sim 1$ –1.5. Fainter optical objects with $\log\ S_{15}/S_{r'} \sim 3$ have typically larger luminosities $L > 10^{13}\ L_{\odot}$, redshifts $z \sim 1.3$ and reddening $A_v \sim 2$. Luminous AGN, with $L \sim 10^{12}\ L_{\odot}$, also populate this area.

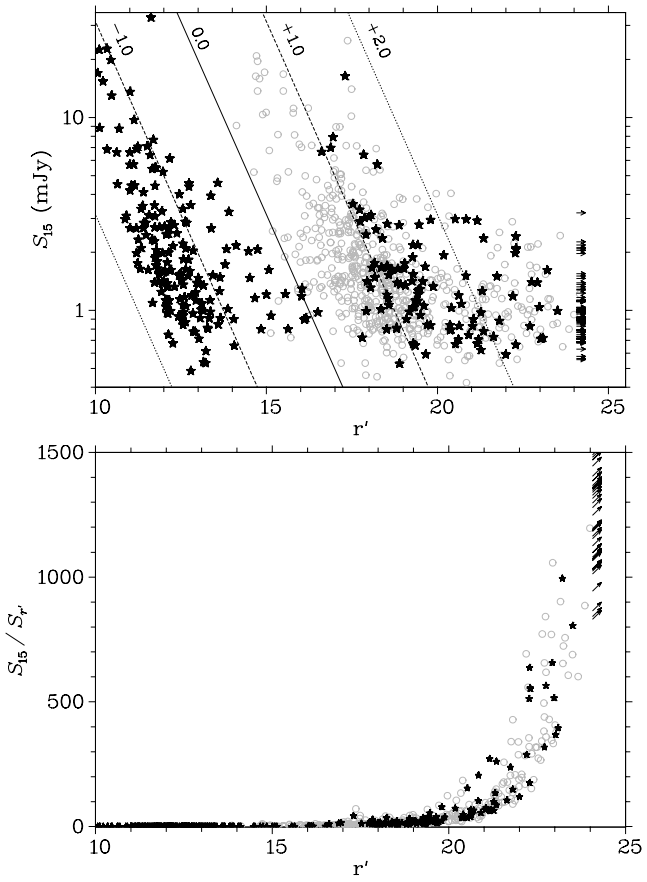

Figure 6. Optical to IR flux ratio for 15-μm sources with optical counterpart. Top figure shows the mid-IR flux versus optical magnitude. Point-like classified object are shown as black stars while galaxies are shown as grey circles. The lines of constant flux ratio $\log(S_{15}/S_{r'}) = -1.0$, 0.0, +1.0, +2.0 are also shown. Blank fields are displayed using a right arrow. Bottom figure shows $\log(S_{15}/S_{r'})$ versus optical magnitude.

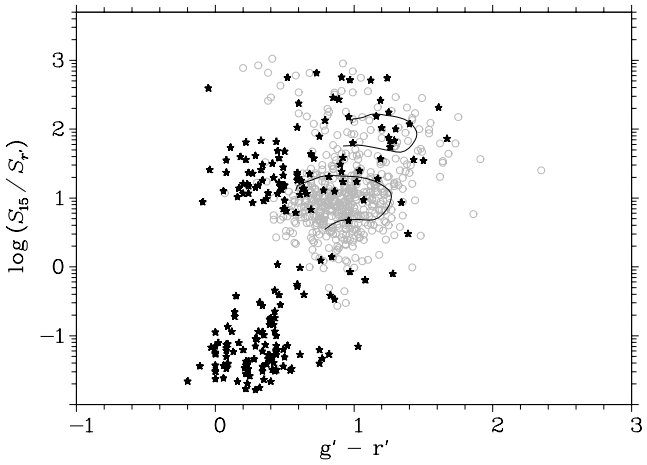

Figure 7. IR to optical flux ratio versus optical colour $g' - r'$. Symbols as in Fig. 6. The lower left point-like objects are Galactic stars. The solid lines show the locus of normal star forming galaxies (lower track) and Arp220 objects (upper track).

The association of this sources with very reddened objects supports the assumption that the objects with $S_{15}/S_{r'} > 100$ in Fig. 6 may represent a population of highly obscured luminous and ultra-luminous starburst galaxies and AGNs.

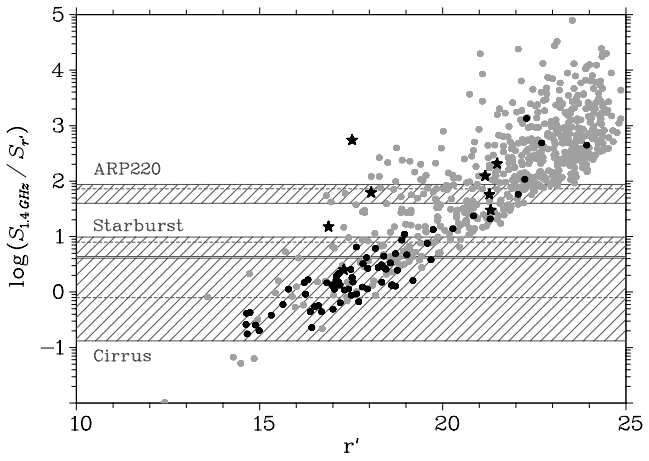

Figure 8. Radio to optical flux ratio versus optical magnitude. The black symbols represent the sources detected also at 15 μm (dots, galaxies; stars, point-like objects). Hatched areas represent the range predicted by different IR galaxy types in the range $0 < z < 1.5$ (redshift increases from bottom to top in each area; dashed line shows the location of $z = 1.0$).

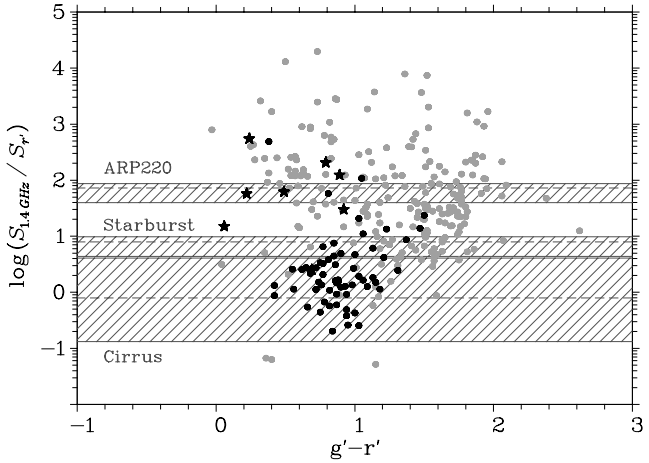

Figure 9. Radio to optical flux ratio versus optical colour. Symbols as in Fig. 8.

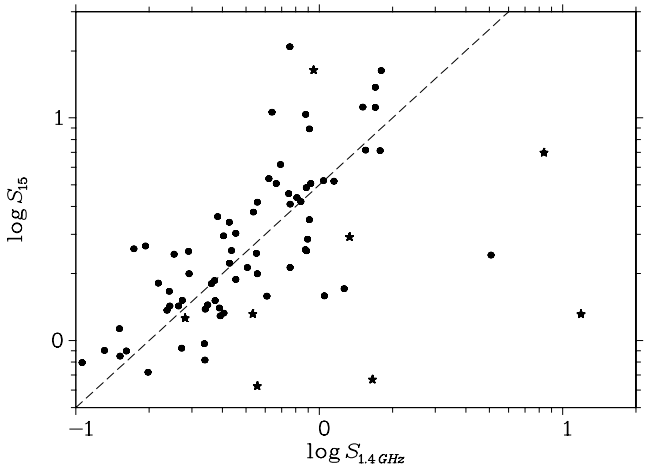

Figure 10. Mid-IR flux versus radio flux (mJy). The black dots represent objects classified as galaxies and the black stars those classified as point-like.

7 SUMMARY

The association of sources detected at 15 μm in the ELAIS N1 and N2 areas with optical objects is presented. A 92 per cent of the sample presents an optical identification to $r' = 24$. The magnitude distribution presents a maximum at $r' = 18$ and a tail which extends to fainter magnitudes. The distribution of point-like objects presents a maximum 1 mag fainter. The mid-IR to optical flux ratios, $S_{15}/S_{r'}$, of the bright optical sources are in the range 1–10^2 and can be explained using simple models of cirrus, starbursts, AGN and Arp220 SEDs. The tail of faint objects, show larger $S_{15}/S_{r'}$ values, from 10^2 to 10^3 and can only be explained assuming large luminosities and obscurations. Point-like objects show bluer $g' - r'$ colour with higher mid-IR to optical flux ratio than galaxies. The remaining 8 per cent of objects not identified are faint in the mid-IR , with a 15-μm flux lower than 3 mJy. However, their mid-IR-to-optical flux ratio is larger than 10^3 favouring the interpretation that they are associated with starbursts or AGNs at high redshifts and highly obscured. The identification of radio sources in the same areas is also presented. Their magnitude distribution shows an increase in the number of sources towards faint magnitudes. The proportion of unidentified objects is 44 per cent.

These results are in agreement with those obtained in the ELAIS southern areas as presented by Pozzi et al. (2003) and La Franca et al. (2004) but extends the sample to a larger number of objects and their identifications to fainter optical magnitudes.

ACKNOWLEDGMENTS

EAGS aknowledges support by EC Marie Curie Fellowship MCFI-2001-01809 and PPARC Grant No. PPA/G/S/2000/00508. The ELAIS consortium also acknowledges support from EC Training Mobility Research Networks '*ISO* Survey' (FMRX-CT96-0068) and 'Probing the Origin of the Extragalactic background light (POE)' (HPRN-CT-2000-00138) and from PPARC. This paper is based on observations with *ISO*, an ESA project, with instruments funded by ESA Member States (especially the PI countries: France, Germany, the Netherlands and the United Kingdom) and with participation of ISAS and NASA. The INT is operated on the island of La Palma by the Isaac Newton Group in the Spanish Observatorio del Roque de los Muchachos of the Instituto de Astrofisica de Canarias.

REFERENCES

Abazajian M. et al., 2003, AJ, 126, 2081
Aussel H., Cesarsky C. J., Elbaz D., Starck J. L., 1999, A&A, 342, 313
Bertin E., Arnouts S., 1996, A&AS, 117, 393
Calzetti D., Armus L., Bohlin R. C., Kinney A. L., Koornneef J., Storchi-Bergmann T., 2000, ApJ, 533, 682
Cesarsky C. J. et al., 1996, A&A, 315, L32
Ciliegi P. et al., 1999, MNRAS, 302, 222
Fadda D., Flores H., Hasinger G., Franceschini A., Altieri B., Cesarsky C. J., Elbaz D., Ferrando P., 2002, A&A, 383, 838
Flores H. et al., 1999, ApJ, 517, 148
Genzel R., Cesarsky C. J., 2000, ARA&A, 38, 761
Greisen E. W., Calabretta M. R., 2002, A&A, 395, 1061
Gruppioni C., Lari C., Pozzi F., Zamorani G., Franceschini A., Oliver S., Rowan-Robinson M., Serjeant S., 2002, MNRAS, 335, 831
Irwin M., Lewis J., New Astron. Rev., 45, 105
Kessler M. F. et al., 1996, A&A, 315, L27
La Franca F. et al., 2004, AJ, 127, 3075

Landolt A., 1992, AJ, 104, 340
Lari C. et al., 2001, MNRAS, 325, 1173
Lemke D. et al., 1996, A&A, 315, L64
McMahon R. G., Walton N. A., Irwin M. J., Lewis J. R., Bunclark P. S., Jones D. H., 2001, New Astron. Rev., 45, 97
Mann R. G. et al., 1997, MNRAS, 289, 482
Monet D. G., 1998, Bull. Am. Astron. Soc., 30, 1427
Oliver S. et al., 2000, MNRAS, 316, 749
Oliver S. et al., 2002, MNRAS, 332, 536
Pozzi F. et al., 2003, MNRAS, 343, 1348
Rowan-Robinson M., 2001, New Astron. Rev., 45, 631
Rowan-Robinson M. et al., 2004, MNRAS, 351, 1290
Sutherland W., Saunders W., 1992, MNRAS, 259, 413
Vaccari M., et al., 2005, MNRAS, in press (doi: 10.1111/j.1365-2966.2005.08733.x) (astro-ph/0404315)
Willott C. J. et al., 2003, MNRAS, 339, 397
York D. G. et al., 2000, AJ, 120, 1579

This paper has been typeset from a TEX/LATEX file prepared by the author.